Processing and Application of Ceramics 14 [4] (2020) 362–371
https://doi.org/10.2298/PAC2004362A

Experimental and *ab initio* study of the structural and optical properties of ZnO coatings: Performance of the DFT+*U* approach

Agustín Apaolaza[1], Diego Richard[1,2], Matías R. Tejerina[2,3,*]

[1]*Facultad de Ciencias Exactas, Universidad Nacional de La Plata (UNLP), calle 115 y 47 (1900) La Plata, Argentina*
[2]*Centro de Tecnología de Recursos Minerales y Cerámica (CETMIC), CIC-CONICET, Camino Centenario y 506, CC 49 (B1897ZCA) M.*
[3]*Facultad de Ingeniería, Universidad Nacional de La Plata (UNLP), Av 1 y 47 (1900) La Plata, Argentina*

Received 8 May 2020; Received in revised form 5 October 2020; Accepted 31 October 2020

Abstract

In this work, ZnO coatings were produced by the spray-pyrolysis technique and characterized by scanning electron microscopy, X-ray diffraction and optical transmittance spectroscopy. The experimental results were compared to predictions obtained from electronic-structure calculations based on the Density Functional Theory plus U (DFT+U) approach. To this purpose, the 2H, 4H and 6H polytypes of ZnO were theoretically analysed, and DFT+U was assessed for the calculation of structural, electronic and optical properties of the hexagonal ZnO structures. We found that DFT+U is an effective and accurate method that combined with experimental measurements, allows a deeper insight about the coatings of the wurtzite (2H) phase synthesized in the laboratory. This comprehensive study of the pure ZnO is the first step towards the study of more complex ZnO-based coatings.

Keywords: *ZnO, structure, optical properties, electronic-structure calculations*

I. Introduction

Zinc oxide (ZnO) is an important semiconductor with broad applications in technological devices such as solar cells, optical filters, and gas sensors, among many others [1–3]. Processed as thin films and coatings, ZnO is widely studied for applications in optoelectronics [4–7]. To enhance material performance in such applications, the study of its elastic and optical properties is of paramount importance. In this sense, in the last decade many experimental investigations have addressed the different structural and optical properties of pure and doped ZnO systems [3–18]. As a general remark, these investigations frequently report how the material band gap energy (E_g) and its elastic moduli depend on different parameters related to the processing method.

On the other hand, the theoretical description of the ZnO properties using computational methods based on Density Functional Theory (DFT) presents some challenges. In particular, it is well known that the prediction of E_g using the most common approximations for the exchange and correlation energy underestimates the experimental value (the "band gap problem" [19,20]). Considering this, many DFT approaches have been proposed to improve the predictions of E_g in ZnO, and related electronic properties [20–26]. Among them, the semiempirical methods that include a Hubbard parameter U in orbitals of the constituent atoms of the system (DFT+U approach) have demonstrated to be accurate in predicting these electric properties of ZnO and less computationally expensive than other methods [20,24–29]. In this case, the choice of the U parameter requires detailed studies of its incidence in other properties of ZnO besides E_g [24,25,27,30]. Based on its good performance in the pure compound, the DFT+U approach has also been proposed to model the case of ZnO doped with transition metals and lanthanide atoms [28,29,31–36]. So, nowadays, investigations that combine experimental determinations and DFT+U predictions are quite common, because this combination allows a deeper understanding of the materials through the relation of the

*Corresponding author: tel: +54 0221 484 0167 (121),
e-mail: *matiast@cetmic.unlp.edu.ar*

observed properties and the modelling of their origins [34,36–40].

In this work, we analyse the performance of the DFT and DFT+U methods to simultaneously describe the structural, electronic and optical properties of the 2H, 4H and 6H polytypes of ZnO. We aim to assess the DFT+U method as a tool for predicting and describing the different properties of wurtzite ZnO phase coatings prepared by spray-pyrolysis (SP) in the laboratory. To the best of our knowledge, the implementation of DFT+U method to analyse the 4H and 6H polytypes is reported for the first time. In this paper, we firstly present a characterization of the SP manufactured ZnO coatings. To this end, scanning electron microscopy (SEM), X-ray diffraction (XRD), and optical transmittance spectroscopy were employed. Then, we have performed a wide range of DFT and DFT+U predictions for the properties in polytypes of bulk ZnO and we compare them with the results obtained for the manufactured coatings and also with the literature. Hence, we investigated the electronic and optical properties by performing measurements and calculations of the transmittance spectra and E_g. Regarding the structure, we covered different scales of the ZnO system, going from the crystallographic structure (lattice parameters, elastic constants) to the atomic local environments. In this respect, we focused on the electric field gradient (EFG) at each atomic site of the structure because it is highly sensitive to small changes in the electronic charge density close to that site. Then, the EFG is a very good indicator of the prediction accuracy at the nanoscopic scale.

All these structural and electronic properties are of interest in the fabrication processes of ZnO-based thin films and coatings. Moreover, this comprehensive analysis of the ZnO properties, by combining experimental and *ab initio* techniques, is important as a key starting point for future research in more complex ZnO-based materials, such as doped ZnO coatings.

II. Materials and methods

2.1. Experimental procedure

The ZnO coatings were produced by spray pyrolysis (SP) starting from a precursor solution containing zinc acetate dihydrate (ZAD), acetylacetone (AcA) as a stabilizer and ethanol as a solvent [41]. The precursor solution was prepared by dissolving 5 g of ZAD in a mixture composed of 50 ml of ethanol and 5 ml of AcA. Then, the sol was stirred for 30 min at room temperature. For the SP coatings, microscope soda-lime glass slides were used as substrates, which were previously washed with a detergent solution, ethanol, acetone and dried at 80 °C. The precursor solution was manually atomized through a conventional airbrush, using 3.0 bar pressurized air. The application onto the glass substrate, heated at 450 °C, was carried out in three steps to generate zones of different thickness (called Z1, Z2 and Z3). At first, 19.0 ml of the solution was applied over the whole substrate surface, then the substrate was partially masked leaving two thirds free, and the other 19.0 ml of solution was applied over the uncovered region. After this, the procedure was repeated, we covered half of the remaining surface and applied 13.4 ml of the solution to the exposed surface (one-third of the total surface). As a result, the region Z1 was sprayed with 6.3 ml, the region Z2 with 15.8 ml and Z3 with 29.2 ml of the solution, so different thicknesses were obtained over the same substrate. This could be confirmed with naked-eye inspection (Fig. 1).

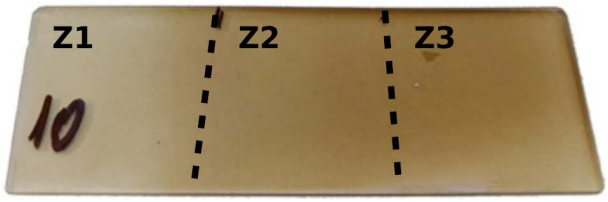

Figure 1. Image of ZnO coatings onto the substrate with three zones: Z1, Z2, and Z3

The resulting coatings were characterized by SEM (JEOL JCM-6000 instrument), XRD (BRUKER D2 Phaser instrument), and optical transmittance spectroscopy (Cary 5000, Agilent Technologies). These measurements allowed an analysis of the coating thickness and morphology at the micrometric scale, its crystal structure and the estimation of E_g.

2.2. Ab initio calculations

We performed all our calculations with the open-source Quantum Espresso (QE) package, which is based on pseudopotentials and plane waves [42]. Generalized gradient approximation (GGA) exchange-correlation functional has been used, with the Perdew-Burke-Ernzerhof (PBE) parametrization [43].

As the starting ZnO structures, we considered those of the wurtzite (2H) type reported by Wyckoff [44], which is available at the crystallography open database (COD ID 9008877) [45], and the 4H and 6H polytypes reported by Zagorac *et al.* [22]. The 2H structure contains two formula units per unit cell, and the Zn atoms are tetrahedrally coordinated with O atoms (Fig. 2a). The 4H and 6H correspond to stacking variants of the wurtzite structure (Figs. 2b and 2c). They were recently reported as theoretical stable structures of ZnO that may allow a fine-tune of electronic properties [21,22,46]. The three structures were fully optimized at DFT and DFT+U levels. For the last, the PBE functional was complemented by adding *ad hoc* Hubbard potentials on the d orbitals of Zn atoms and the p orbitals of O atoms. Considering previous investigations, we used U parameters of 12 and 6.5 eV for Zn and O, respectively [25,27,29].

Calculations were performed using a Monkhorst-Pack grid of $6 \times 6 \times 6$ k-points and a kinetic energy cutoff of 100 Ry. The optimized structures were obtained by minimizing the total energy as a function of the lat-

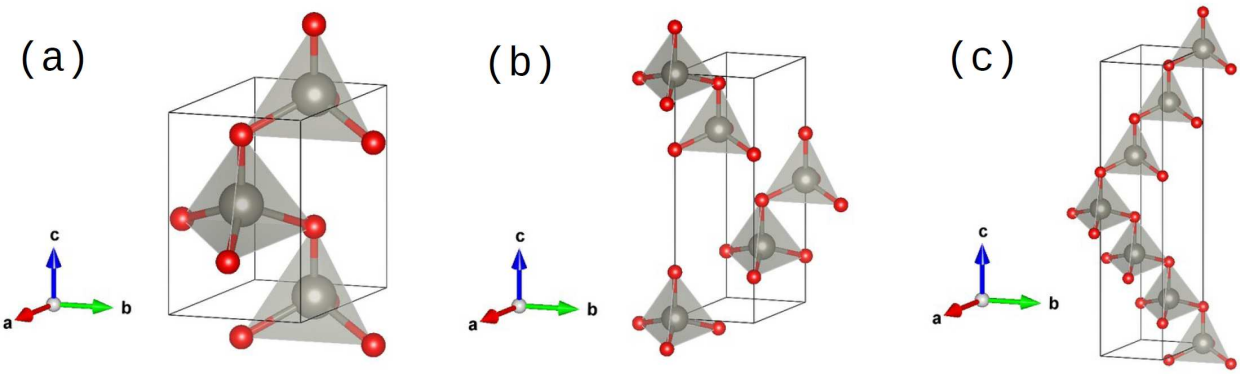

Figure 2. Visualization of the experimentally observed wurtzite (2H) type (a) and the theoretically calculated 4H polytype (b) and 6H polytype (c) modifications of ZnO (the grey and red spheres stand for the Zn and O atoms, respectively)

tice parameter a and the c/a ratio [47], and allowing the atoms to relax until the forces on them were 0.025 eV/Å or less.

For the three optimized structures the electronic and optical properties were analysed by calculating the density of electronic states (DOS) and the dielectric function $\varepsilon(\omega)$ and its optical related properties: the absorption coefficient $\alpha(\lambda)$, the real part of the refractive index $n(\lambda)$, and the transmittance spectra $T(\lambda)$ [28,29,42].

On the other hand, by considering that among the three studied ZnO polytypes, the 2H bulk phase is the one reported experimentally, additional properties were predicted for this structure to make a comparison with previously published results. In this sense, the Zn and O local environments were analysed by considering variations in the Zn–O distances and studying the EFG at the Zn and O sites. For this purpose, we used the Gauge-Included Projector Augmented Waves (GIPAW) approach [42,48,49]. Finally, from a set of strains applied to the DFT and DFT+U equilibrium structures, the elastic constants C_{ij} and the bulk modulus B were calculated [47,50].

III. Results

3.1. Experimental results

SEM images obtained for the sample Z3 after polishing one face of this sample up to optical quality (1/4 μm) are presented in Fig. 3. As it can be seen, the local measurement of the sample thickness gives about 1.5 μm at the end-face. Also, pores or inhomogeneities were observed at the micrometric scale, distributed over the film surface and volume (see the dark regions of about 1 μm^2 shown by enclosed curve A in Fig. 3).

XRD pattern of the sample Z3 is shown in Fig. 4a and allows determination of the crystal structure and the coatings preferred orientation. All the sharp diffraction peaks were assigned to the hexagonal phase (wurtzite). We performed a Rietveld refinement considering a preferred directional growth along (002) and (101) planes, and determined the lattice parameters $a = b = 3.2577(6)$ Å, $c = 5.21456(9)$ Å ($c/a = 1.6007(3)$), and the positional parameter $u = 0.3799(1)$, which define the z coordinates of the O atoms in the structure. By using these values the distances from Zn to the apical and basal O atoms were calculated: $d_{(\mathrm{Zn-O_a})} = 1.981(3)$ Å and $d_{(\mathrm{Zn-O_b})} = 1.982(1)$ Å, respectively.

XRD patterns of the coatings Z1, Z2 and Z3 for the selected 2θ range from 30° to 38° are shown in Fig. 4b. In this region, we observed the 002 and 101 diffraction peaks, and also the very weak peak corresponding to (100) plane. As it can be seen, it is clear that the Z1 coating is oriented along (002) plane, which means a preferred growth direction along the c-axis for this sample. On the other hand, the samples Z2 and Z3 have a 101 diffraction peak with higher intensity than the 002 one, which is related to a preference for the (101) plane as the sample thickness increases, as also observed by other authors [51].

The preferential crystallite orientation can be quantitatively analysed with the texture coefficient (TC), which compares the relative peak intensities with those of the reference data card (JCPDS 00-036-1451). The

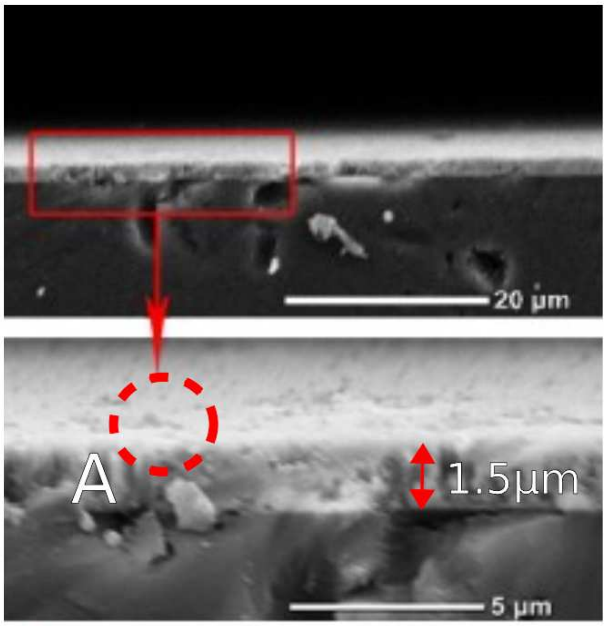

Figure 3. SEM images of the end face of the sample Z3

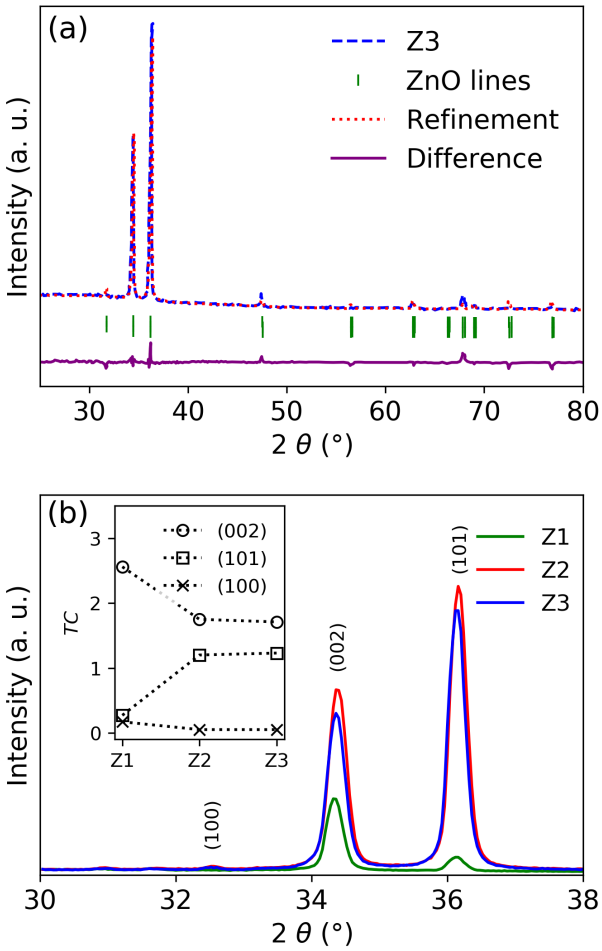

Figure 4. XRD pattern with Rietveld refinement for sample Z3 (a) and detail of the (100), (002) and (101) diffraction peaks (b) for samples Z1, Z2 and Z3 and texture coefficients *TC* (inset)

TC factor was estimated using the following relation:

$$TC_{(hkl)} = \frac{\frac{I_{hkl}}{I^0_{hkl}}}{\frac{1}{N}\sum\left(\frac{I_{hkl}}{I^0_{hkl}}\right)} \quad (1)$$

where $TC_{(hkl)}$ corresponds to the *hkl* plane, I is the measured peak intensity, I^0 the corresponding one of the reference card, and N is the number of considered reflection faces in the XRD pattern. The deviation of TC from unity implies the film growth in a preferred orientation. The TC values for the (002), (101), and (100) planes are shown in inset of Fig. 4b. As it can be seen, the Z1 has the highest $TC_{(200)}$ value, being 2.7, and it is about 1.5 for the Z3 and Z2 coatings. The opposite behaviour was observed for $TC_{(101)}$, being about 0.2 for the Z1 and increasing up to 1.2 for both Z2 and Z3 coatings, whereas $TC_{(001)}$ is about 0.1–0.2 in all three samples.

Regarding the optical properties, Fig. 5 shows the transmittance spectra of the Z1, Z2 and Z3 coatings. As it can be seen, the thicker coatings present more interference fringes. The maximum transmittance (about 90%) is obtained in the infrared (IR) region, whereas at the visible range the transmittance is between 40 and 80%. The inhomogeneities observed by SEM are represented in these measurements by the shrinkage of the two evolving curves: one that interpolates maximums and the other that interpolates minimum values of interference fringes (dashed lines around Z3 transmittance in Fig. 5), i.e. an important reduction of the oscillation amplitude is observed as wavelength decreases [52]. From the interference fringes in the λ range of 700–1000 nm, we determined the coating thickness t. To this purpose, we compared the experimental spectra with simulations of $T(\lambda)$ obtained using the widely known Filmetrics reflectance calculator based on the complex-matrix form of the Fresnel equations [53]. By considering coatings with a refractive index n between 1.8 and 2.0 [5,7,8], and a SiO_2 substrate with $n_s = 1.45$, we obtained $t = 1.3(1)$, $2.1(1)$, and $2.3(1)$ µm for samples Z1, Z2, and Z3, respectively. For Z3, the difference of the t value with the local thickness of about 1.5 µm observed by SEM (Fig. 3) can be attributed to the variation of thickness along the sample surface.

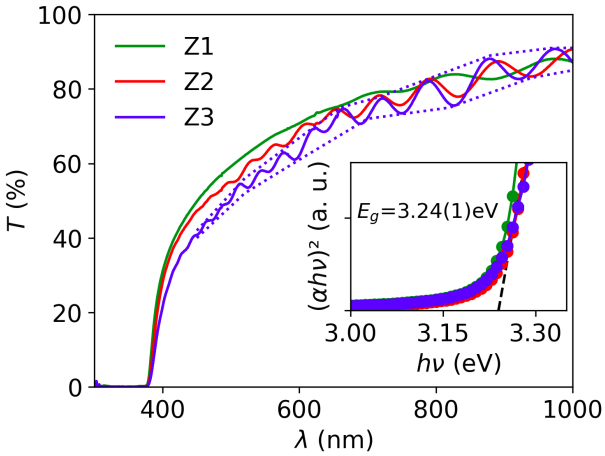

Figure 5. Transmittance spectra and Tauc's plot (inset)

On the other hand, to determine the optical band gap E_g, we used the Tauc's relation $\alpha h\nu = A(h\nu - E_g)^{1/2}$, where A is a constant, $h\nu$ is the photon energy, and the absorption coefficient α is calculated from the transmittance $T(\lambda)$ using the Beer-Lambert law $\alpha = \ln(1/T)/t$. The Tauc's plots $(\alpha h\nu)^2$ vs. $h\nu$, presented in inset of Fig. 5, were used to determine E_g by extrapolating the linear portion to zero. It was found that $E_g = 3.24(1)$ eV for all three samples, a value that is in good agreement with the results reported for ZnO films by other authors [8,10,12,13].

3.2. Calculation results

DFT and DFT+U optimized structures

Table 1 summarizes the basal lattice parameter a and the c/a ratio for 2H, 4H and 6H polytypes obtained using the DFT and DFT+U approaches. For comparison, other theoretical data available in the literature for all three polytypes were also included [21,22] together with

Table 1. Lattice parameters for ZnO polytypes obtained by DFT and DFT+U (for three polytypes, theoretical values predicted by other authors are also included as well as the experimental values for ZnO bulk and coating)

Method	a [Å]	c/a
	Structure type 2H	
DFT	3.3169	1.6087
DFT+U	3.2764	1.6043
Exp. (Wyckoff [44])	3.2495	1.6024
Exp. (this work)	3.2577(6)	1.6007(3)
Theor. GGA [21]	3.2855	1.6137
Theor. LDA [22]	3.19	1.6238
Theor. B3LYP [22]	3.28	1.6128
	Structure type 4H	
DFT	3.2501	3.2466
DFT+U	3.2156	3.2437
Theor. GGA [21]	3.2775	3.2488
Theor. LDA [22]	3.19	3.2539
Theor. B3LYP [22]	3.28	3.2439
	Structure type 6H	
DFT	3.2460	4.8886
DFT+U	3.2003	4.9668
Theor. GGA [21]	3.2752	4.8822
Theor. LDA [22]	3.18	4.8838
Theor. B3LYP [22]	3.27	4.8962

the experimental results reported by Wyckoff [44] and data obtained in this work for the 2H phase.

Our calculations show that the different polytypes have a similar basal lattice parameter. The predicted a and c/a values are in good agreement with the available experimental and theoretical data. As it can be seen in Table 1, the optimization of the 2H structure leads to a slight overestimation of the lattice parameters (up to about 2% of the experimental values). A closer look at these results shows that the inclusion of the Hubbard term produces lattice parameters closer to the experimental ones. This improvement in the prediction of the 2H unit cell with DFT+U was also observed before by other authors [23,24,26].

DOS, bandgap and optical properties

The results of the density of electronic states (DOS) corresponding to the different ZnO structures and calculation approaches are shown in Fig. 6. As it can be seen, for the same calculation method (DFT or DFT+U) no significant changes of the DOS are observed from one cell to another. For the 2H type, the DOS corresponding to the starting structure (dashed lines in Fig. 6) is also presented to show that the structural optimizations do not produce significant changes in the electronic properties. In general, the DOS presents the valence band with O-2p and Zn-4d character, separated from the Zn-2s conduction band by E_g. In the case of DFT calculations (Fig. 6a), we obtained E_g values of about 1 eV, which underestimates the experimental value and reflects the well-known band gap problem. The addition of the U parameter modifies the DOS and increases the predicted E_g to about 3.4 eV (Fig. 6b), which is in better agreement with the measured band gaps.

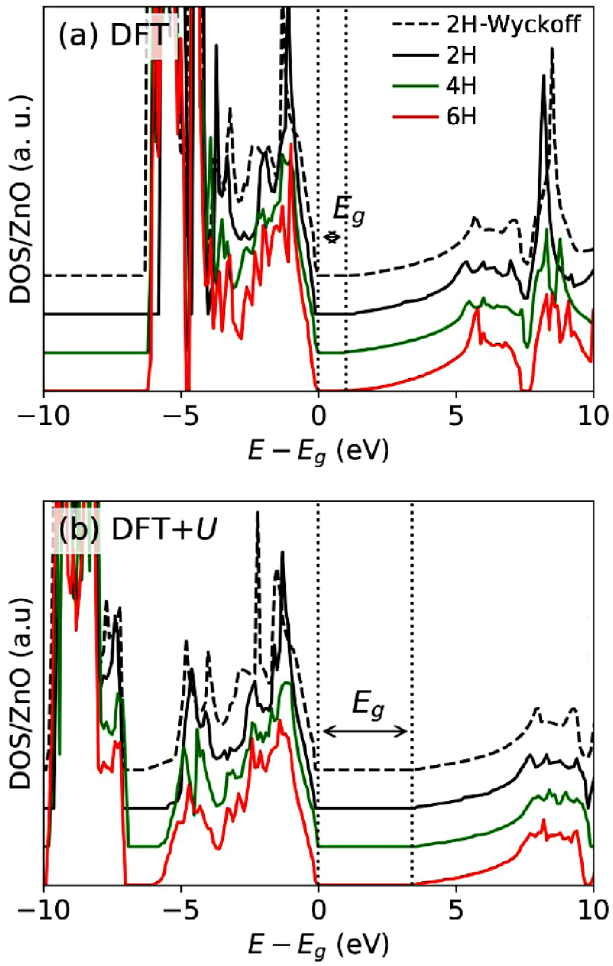

Figure 6. DOS calculated for the different structures according to the DFT (a) and DFT+U methods (b) (the scale of energy refers to the Fermi level and the extent of E_g is indicated between the vertical dotted lines)

Considering the improvement obtained with DFT+U, we used this approach to calculate the dielectric function $\varepsilon(\omega)$ and related optical properties. The real and imaginary part of $\varepsilon(\omega)$ (ε_1 and ε_2, respectively) for all three structures are given in Fig. 7a. As it can be seen again, no significant changes in these dielectric functions are observed from one polytype to another. These results show the typical behaviour for a semiconductor: ε_1 is a positive function, which approaches the dielectric constant ε_∞ in the limit $\omega \rightarrow 0$ (experimentally, $\varepsilon_\infty = 3.7$ [16,54]). On the other hand, the first ε_2 slight shoulder at about 3.4 eV corresponds to the interband absorption edge in the range of UV energies, expected according to the transparency of the ideal ZnO [29,30,54]. By using $\varepsilon_1(\omega)$ and $\varepsilon_2(\omega)$, we calculated $\alpha(\lambda)$ and $n(\lambda)$ [28] (Fig. 7b). Our predictions for all these optical properties are in good agreement with previous calculations by other DFT methods [20,26,31,33,55], as well as with the experimental measurements obtained

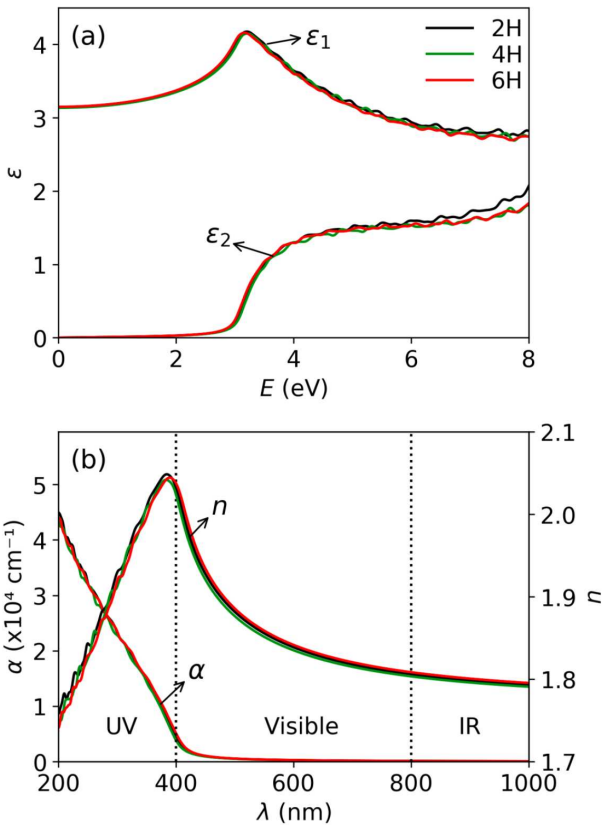

Figure 7. Dielectric function $\varepsilon = \varepsilon_1 + j\varepsilon_2$ (a) and absorption coefficient α and the real part of the refractive index n (b) for different fully optimized ZnO structures with DFT+U

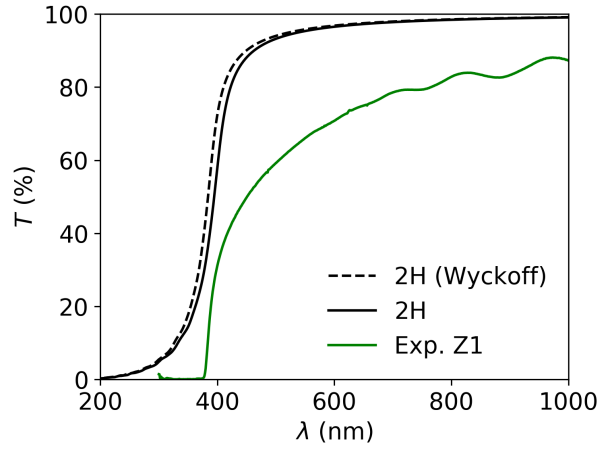

Figure 8. DFT+U simulated transmittance spectra T in the range of 200–1000 nm for the 2H type ZnO, before and after structural optimization, and comparison with experimental measurement for the Z1 sample

for thin films and bulk ZnO possessing the wurtzite phase [8,54].

Finally, we used the calculated absorption coefficient to simulate the transmittance spectra $T(\lambda) = \exp(-\alpha(\lambda)t)$ for the 2H structure, using a thickness $t = 1.3\,\mu m$. The obtained results are presented in Fig. 8 and we compared them with the experimental spectrum corresponding to the sample Z1. The predicted $T(\lambda)$ does not significantly depend on the considered lattice parameters and internal coordinates, as it can be seen from the similar spectra obtained using the 2H starting structure of Wyckoff [44] and the DFT+U fully optimized in this work. On the other hand, differences from the experimental spectrum can be attributed to finite thickness, surface roughness, and sample inhomogeneity and porosity, which affect the optical transmittance, especially in the visible range [13,52].

Local structures and EFGs in wurtzite (2H) ZnO

Considering that among the three polytypes only the wurtzite phase of ZnO is known experimentally, and it was the one observed in our ZnO coatings, further DFT and DFT+U studies were performed for this structure. As presented in Fig. 2a, the Zn atoms are tetrahedrally coordinated with O atoms, so the atomic environments can be characterized by the distances from the Zn atom to the apical and the basal oxygen atoms ($d_{(Zn-O_a)}$ and $d_{(Zn-O_b)}$, respectively). These distances before and after the DFT and DFT+U structural optimization are presented in Table 2. As it can be seen, the internal atomic relaxation from the starting structure of Wyckoff [44] to the final ones produces a change of both distances, in a way that the values approach each other, and also to the d values obtained from our XRD measurements. This result suggests that the four O atoms around Zn are located at the corners of a practically regular tetrahedron.

We also analysed the local structures by calculating the EFG because it is a quantity very sensitive to changes in the local environments. The last two columns in Table 2 present the predictions for the largest component of the diagonalized EFG tensor in the principal axis system, V_{zz}, at the Zn and O atomic sites. The tensor is complemented by the asymmetry parameter η, which for the considered wurtzite structure is null at both atomic sites. The obtained results for the EFG show that changes of the Zn–O distances from one cell to another strongly affect the predicted values of V_{zz}. In particular, we found that the structural relaxations must be taken into account to correctly reproduce the exper-

Table 2. Local structures and EFGs for the 2H ZnO unit cells (the experimental values in the last row come from [a] this work, and [b] Ref. [56] and the sign of V_{zz} is unknown)

2H structure		$d_{(Zn-O_a)}$ [Å]	$d_{(Zn-O_b)}$ [Å]	$V_{zz(Zn)}$ [10^{21} V/m^2]	$V_{zz(O)}$ [10^{21} V/m^2]
Starting structure of Wyckoff [44]	DFT	1.796	2.042	−8.13	+2.47
	DFT+U	1.796	2.042	−9.25	+2.53
DFT fully optimized		2.031	2.018	+0.61	−0.26
DFT+U fully optimized		2.000	1.993	+0.60	−0.25
Experimental values		1.981(3)[a]	1.982(1)[a]	0.6595(2)[b]	0.2326(7)[b]

Table 3. Results corresponding to the elastic properties of the 2H structure of ZnO

	C_{11} [GPa]	C_{12} [GPa]	C_{13} [GPa]	C_{33} [GPa]	C_{44} [GPa]	B [GPa]
DFT	204	89	69	207	42	119
DFT+U	244	110	86	243	53	144
GGA [58]	235	67	61	288	50	129
B3LYP [59]	218	124	106	223	44	148
Exp. [60]	209(1.5)	120(1)	104.4(2.0)	216(4)	44.3	143(5)
Exp. [61]	206(4)	116(5)	118(10)	211(4)	44(1)	147(7)

imental values [56]. Therefore, as it can be seen from Table 2, the structural relaxations (involved in the fully optimized structures) are necessary to correctly describe the local structures observed in our XRD measurements and the EFG experimental values. This means that the starting structure considered for our calculations has an incorrect value of u positional parameter and therefore wrong Zn–O distances, as other authors also mentioned [57]. Nevertheless, we included these results to show that DFT and DFT+U can find the correct atomic positions after structural relaxations, and also the correct V_{zz} values. Considering the high sensitivity of the EFG, the comparison of these predicted and measured quantities is very suitable to assess the accuracy of the calculation approaches.

Elastic properties of the wurtzite (2H) ZnO

The elastic constants C_{ij} and the bulk modulus B calculated for the wurtzite structure are presented in Table 3. The Voigt's notation is used according to which $i, j = 1, 2, \ldots, 6$ ($1 = xx$, $2 = yy$, $3 = zz$, $4 = yz$, $5 = xz$, $6 = xy$). In our case, the C_{ij} coefficients are the five independent components of the fourth-rank tensor corresponding to the hexagonal solid [47]. Table 3 also includes theoretical data calculated by other authors using GGA [58] and the hybrid functional B3LYP [59], as well as the available experimental values obtained for ZnO polycrystalline films [60,61]. It can be noted that our predictions are in a general agreement with those values. A comparison of our DFT values with the experimental data shows that the calculated C_{ij} systematically underestimates the experimental value, which is expected according to the systematic overestimation of the equilibrium lattice parameters obtained with DFT (Table 1). The inclusion of the U parameter produces an increase in the predicted C_{ij} values, giving C_{ij} values dispersed around the experimental ones, with differences up to about 30% (for C_{13}). Finally, the bulk modulus B, calculated through a linear combination of the elastic constants [59], follows the same general agreement already described.

IV. Discussion

Even though there are some studies of ZnO-based systems that combine experiments and DFT+U calculations, to the best of our knowledge, there has been no comprehensive analysis of the performance of the DFT+U approach that simultaneously describes structural, optical and elastic properties of ZnO as it has been done in the present investigation, where the *ab initio* predictions are proposed to complement experimental studies on ZnO coatings. Therefore, we produced and characterized ZnO coatings and also we also performed first-principles calculations for three polytypes of hexagonal ZnO. This combination of measurements and predictions allowed us to simultaneously analyse different properties of the synthesized coatings and also to assess the DFT+U method for predicting those properties in the different polytypes. For the experimental existing 2H phase, our systematic comparison of the DFT+U predictions with DFT and experimental results demonstrated that DFT+U is effective to predict and describe not only bandgap energy, as it is already known, but also the structural and elastic properties of ZnO. In this sense, its strength lies in its vast range of applicability: from the atomic local environments (through the Zn–O distances and EFGs) to the crystallographic scale and the elastic constants. Then, the presented combination of calculations and experiments enhances the analysis of the materials. For example, we showed that after considering the structural relaxations the atomic environments have strong differences compared to those of the starting structure, and such relaxations are required to correctly describe the properties observed through XRD and EFG measurements. In contrast, these local environment differences are not reflected by the optical transmittance spectra. So, we can propose interplay between the *ab initio* models and a variety of experimental results to validate the calculation methods and assess the sensitivity of the involved experimental techniques. Considering this, we found that the DFT+U predicted properties are generally in a good agreement with our own experimental measurements performed on the ZnO coatings produced with the SP technique. The few differences between predictions and measurements could be expected according to the method and due to the simplicity of the proposed modelling approach and the complex nature of the real samples. Then, DFT+U is useful to obtain information about the optical and elastic properties of ZnO, which is of practical importance in the design of thin films and coatings.

The present results allow us to extend this methodology to analyse further aspects related to the electro-optical and piezo-optical applications of ZnO coatings. For example, how the film deposition and growing conditions affect the residual stress and C_{ij} coefficients [5,7,12,13,61]. Furthermore, the DFT+U may be ap-

plied to more complex ZnO systems to predict optical and elastic properties when defects, impurities, and interfaces are present [3,4,6,14,22,26].

V. Conclusions

ZnO coatings were produced by the spray-pyrolysis technique and characterized by scanning electron microscopy, X-ray diffraction and optical transmittance spectroscopy. The experimental results were compared to predictions obtained from the electronic-structure calculations based on the DFT+U approach. We consider that this study is a successful first step towards the study of more complex ZnO-based coatings, where the *ab initio* calculations support the experiments to achieve a deeper insight into the material properties, which are central to the development of optically active nanocomponents like diodes, lasers, solar cells and band optical filters.

Acknowledgments: We wish to acknowledge the Argentinian funding institutions for supporting this work: Agencia Nacional de Promoción de Ciencia y Tecnología under contract PICT 2015-0452 and Universidad Nacional de La Plata (UNLP) under grant "Jóvenes Investigadores". Part of the results presented in this work has been obtained using the facilities of the CCT-Rosario Computational Center, member of the High Performance Computing National System (SNCAD, MinCyT-Argentina). We want to thank Dra. Susana Conconi (CETMIC) for assistance with XRD analysis. D. R. and M. R. T. are members of Consejo Nacional de Investigaciones Científicas y Técnicas, CONICET, Argentina.

References

1. P. Rong, S. Ren, Q. Yu, "Fabrications and applications of ZnO nanomaterials in flexible functional devices - A Review", *Crit. Rev. Anal. Chem.*, **49** [4] (2019) 336–349.
2. J. Theerthagiri, S. Salla, R.A. Senthil, P. Nithyadharseni, A. Madankumar, P. Arunachalam, T. Maiyalagan, H.-S. Kim, "A review on ZnO nanostructured materials: Energy, environmental and biological applications", *Nanotechnology*, **30** [39] (2019) 392001.
3. B. Ghanbari Shohany, A. Khorsand Zak, "Doped ZnO nanostructures with selected elements - Structural, morphology and optical properties: A review", *Ceram. Int.*, **46** [5] (2020) 5507–5520.
4. K.D.A. Kumar, R. Thomas, S. Valanarasu, V. Ganesh, M. Shkir, S. AlFaify, J. Thirumalai, "Analysis of Pr co-doped Al:ZnO thin films using feasible nebulizer spray technique for optoelectronic technology", *Appl. Phys. A*, **125** [10] (2019) 712.
5. G. Malik, S. Mourya, J. Jaiswal, R. Chandra, "Effect of annealing parameters on optoelectronic properties of highly ordered ZnO thin films", *Mater. Sci. Semicond. Process.*, **100** (2019) 200–213.
6. F. Baig, M.W. Ashraf, A. Asif, M. Imran, "A comparative analysis for effects of solvents on optical properties of Mg doped ZnO thin films for optoelectronic applications", *Optik*, **208** (2020) 164534.
7. M.-J. Zhao, Z.-T. Sun, C.-H. Hsu, P.-H. Huang, X.-Y. Zhang, W.-Y. Wu, P. Gao, Y. Qiu, S.-Y. Lien, W.-Z. Zhu, "Zinc oxide films with high transparency and crystallinity prepared by a low temperature spatial atomic layer deposition process", *Nanomaterials*, **10** [3] (2020) 459.
8. A. Ashour, M.A. Kaid, N.Z. El-Sayed, A.A. Ibrahim, "Physical properties of ZnO thin films deposited by spray pyrolysis technique", *Appl. Surf. Sci.*, **252** [22] (2006) 7844–7848.
9. R. Navamathavan, K.-K. Kim, D.-K. Hwang, S.-J. Park, J.-H. Hahn, T.G. Lee, G.-S. Kim, "A nanoindentation study of the mechanical properties of ZnO thin films on (0 0 0 1) sapphire", *Appl. Surf. Sci.*, **253** [2] (2006) 464–467.
10. J.H. Cai, G. Ni, G. He, Z.Y. Wu, "Red luminescence in ZnO films prepared by a glycol-based Pechini method", *Phys. Lett. A*, **372** [22] (2008) 4104–4108.
11. P.-F. Yang, H.-C. Wen, S.-R. Jian, Y.-S. Lai, S. Wu, R.-S. Chen, "Characteristics of ZnO thin films prepared by radio frequency magnetron sputtering", *Microelectron. Reliab.*, **48** [3] (2008) 389–394.
12. T.P. Rao, M.C.S. Kumar, S.A. Angayarkanni, M. Ashok, "Effect of stress on optical band gap of ZnO thin films with substrate temperature by spray pyrolysis", *J. Alloys Compd.*, **485** [1-2] (2009) 413–417.
13. T. Prasada Rao, M.C. Santhoshkumar, "Highly oriented (100) ZnO thin films by spray pyrolysis", *Appl. Surf. Sci.*, **255** [16] (2009) 7212–7215.
14. M.-C. Jun, S.-U. Park, J.-H. Koh, "Comparative studies of Al-doped ZnO and Ga-doped ZnO transparent conducting oxide thin films", *Nanoscale Res. Lett.*, **7** [1] (2012) 639.
15. Y. Cherifi, A. Chaouchi, Y. Lorgoilloux, M. Rguiti, A. Kadri, C. Courtois, "Electrical, dielectric and photocatalytic properties of Fe-doped ZnO nanomaterials synthesized by sol gel method", *Process. Appl. Ceram.*, **10** [3] (2016) 125–135.
16. M.B. Bouzourâa, Y. Battie, S. Dalmasso, M.A. Zaïbi, M. Oueslati, A. En Naciri, "Temperature dependent optical properties of ZnO thin film using ellipsometry and photoluminescence", *Superlattices Microstruct.*, **117** (2018) 457–468.
17. D. Richard, M. Romero, R. Faccio, "Experimental and theoretical study on the structural, electrical and optical properties of tantalum-doped ZnO nanoparticles prepared via sol-gel acetate route", *Ceram. Int.*, **44** [1] (2018) 703–711.
18. E.A. Villegas, R. Parra, L. Ramajo, "Integral nanoindentation evaluation of TiO_2, SnO_2, and ZnO thin films deposited via spray-pyrolysis on glass substrates", *J Mater. Sci. Mater. Electron.*, **30** [2] (2019) 1360–1365.
19. S. Lany, A. Zunger, "Assessment of correction methods for the band-gap problem and for finite-size effects in supercell defect calculations: Case studies for ZnO and GaAs", *Phys. Rev. B*, **78** [23] (2008) 235104.
20. K. Bashyal, C.K. Pyles, S. Afroosheh, A. Lamichhane, A.T. Zayak, "Empirical optimization of DFT+U and HSE for the band structure of ZnO", *J. Phys. Condens. Matter*, **30** [6] (2018) 065501.
21. Z. Huang, T.-Y. Lü, H.-Q. Wang, J.-C. Zheng, "Thermoelectric properties of the 3C, 2H, 4H, and 6H polytypes of the wide-band-gap semiconductors SiC, GaN, and ZnO", *AIP Advances*, **5** (2015) 097204.
22. D. Zagorac, J.C. Schoen, J. Zagorac, M. Jansen, "Theoretical investigations of novel zinc oxide polytypes and in-depth study of their electronic properties", *RSC Adv.*,

5 (2015) 259290.
23. G.-Y. Huang, C.-Y. Wang, J.-T. Wang, "Detailed check of the LDA+U and GGA+U corrected method for defect calculations in wurtzite ZnO", *Comput. Phys. Commun.*, **183** [8] (2012) 1749–1752.
24. M.K. Yaakob, N.H. Hussin, M.F.M. Taib, T.I.T. Kudin, O.H. Hassan, A.M.M. Ali, M.Z.A. Yahya, "First principles LDA+U calculations for ZnO materials", *Integr. Ferroelectr.*, **155** [1] (2014) 15–22.
25. E.S. Goh, J.W. Mah, T.L. Yoon, "Effects of Hubbard term correction on the structural parameters and electronic properties of wurtzite ZnO", *Comp. Mater. Sci.*, **138** (2017) 111–116.
26. K. Harun, N.A. Salleh, B. Deghfel, M.K. Yaakob, A.A. Mohamad, "DFT+U calculations for electronic, structural, and optical properties of ZnO wurtzite structure: A review", *Results Phys.*, **16** (2020) 102829.
27. A. Calzolari, M.B. Nardelli, "Dielectric properties and Raman spectra of ZnO from a first principles finite-differences/finite-fields approach", *Sci. Rep.*, **3** (2013) 2999.
28. Q.-B. Wang, C. Zhou, J. Wu, T. Lü, "A GGA+U study of the optical properties of vanadium doped ZnO with and without single intrinsic vacancy", *Opt. Commun.*, **297** (2013) 79–84.
29. A. Calzolari, A. Ruini, A. Catellani, "Transparent conductive oxides as near-IR plasmonic materials: The case of Al-doped ZnO derivatives", *ACS Photonics*, **1** [8] (2014) 703–709.
30. S.Zh. Karazhanov, P. Ravindran, U. Grossner, A. Kjekshus, H. Fjellvåg, B.G. Svensson, "Strong Coulomb correlation effects in ZnO", *Solid State Commun.*, **139** [8] (2006) 391–396.
31. P. Palacios, I. Aguilera, P. Wahnón, "Electronic structure and optical properties in ZnO:M(Co, Cd): Effect of band-gap variation", *Thin Solid Films*, **518** [16] (2010) 4568–4571.
32. Y.-S. Lee, Y.-C. Peng, J.-H. Lu, Y.-R. Zhu, H.-C. Wu, "Electronic and optical properties of Ga-doped ZnO", *Thin Solid Films*, **570** (2014) 464–470.
33. H.-C. Wu, H.-H. Chen, Y.-R. Zhu, "Effects of Al-impurity type on formation energy, crystal structure, electronic structure, and optical properties of ZnO by using Density Functional Theory and the Hubbard-U method", *Materials*, **9** [8] (2016) 647.
34. S. Horzum, E. Torun, T. Serin, F.M. Peeters, "Structural, electronic and optical properties of Cu-doped ZnO: experimental and theoretical investigation", *Philos. Mag.*, **96** [17] (2016) 1743–1756.
35. M.V. Gallegos, C.R. Luna, M.A. Peluso, L.C. Damonte, J.E. Sambeth, P.V. Jasen, "Effect of Mn in ZnO using DFT calculations: Magnetic and electronic changes", *J. Alloys Compd.*, **795** (2019) 254–260.
36. R. Amari, B. Deghfel, A. Mahroug, A.A. Mohamad, A. Boukhari, N. Selmi, "Effects of Mn doping on the structural, morphological, electronic and optical properties of ZnO thin films by sol-gel spin coating method: An experimental and DFT+U study", *Physica B Condens. Matter*, **577** (2020) 411766.
37. L. Honglin, L. Yingbo, L. Jinzhu, Y. Ke, "Experimental and first-principles studies of structural and optical properties of rare earth (RE = La, Er, Nd) doped ZnO", *J. Alloys Compd.*, **617** (2014) 102–107.
38. J.V.N. Sarma, A. Rahman, R. Jayaganthan, R. Chowdhury, D. Haranath, "Al-doped ZnO nanostructured thin films: Density Functional Theory and experiment", *Int. J. Nanosci.*, **14** [04] (2015) 1550015.
39. M. Bououdina, S. Azzaza, R. Ghomri, M.N. Shaikh, J.H. Dai, Y. Song, W. Song, W. Cai, M. Ghers, "Structural and magnetic properties and DFT analysis of ZnO:(Al,Er) nanoparticles", *RSC Adv.*, **7** [52] (2017) 32931–32941.
40. J.C.A. Queiroz, J.B. Azevedo Filho, J.Q. Medeiros Neto, I. Oliveira Nascimento, I.A. Souza, M.G. Oliveira Queiroz, E.B. Melo, T.H. Carvalho Costa, "Structural and optical properties of Al-doped ZnO thin films produced by magnetron sputtering", *Process. Appl. Ceram.*, **14** [2] (2020) 119–127.
41. G. Suarez, F.C. Alvira, R. Parra, M.R. Tejerina, "Characterization of thin coatings based on ZnO for photonic applications", *Optoelectron. Adv. Mater.*, **13** [9-10] (2019) 535–538.
42. P. Giannozzi, O. Andreussi, T. Brumme, O. Bunau, M. Buongiorno Nardelli, M. Calandra, R. Car, C. Cavazzoni, D. Ceresoli, M. Cococcioni, N. Colonna, I. Carnimeo1, A. Dal Corso, S. de Gironcoli, P. Delugas, R.A. DiStasio Jr., A. Ferretti, A. Floris, G. Fratesi, G. Fugallo, R. Gebauer, U. Gerstmann, F. Giustino, T. Gorni, J. Jia, M. Kawamura, H.-Y. Ko, A. Kokalj, E. Küçükbenli, M. Lazzeri, M. Marsili, N. Marzari, F. Mauri, N.L. Nguyen, H.-V. Nguyen, A. Otero-de-la-Roza, L. Paulatto, S. Poncé, D. Rocca, R. Sabatini, B. Santra, M. Schlipf, A.P. Seitsonen, A. Smogunov, I. Timrov, T. Thonhauser, P. Umari, N. Vast, X. Wu, S. Baroni, "Advanced capabilities for materials modelling with Quantum ESPRESSO", *J. Phys. Condens. Matter*, **29** [46] (2017) 465901.
43. J.P. Perdew, K. Burke, M. Ernzerhof, "Generalized gradient approximation made simple", *Phys. Rev. Lett.*, **77** [18] (1996) 3865–3868.
44. R.W.G. Wyckoff, *Crystal structures, second edition*. Interscience Publishers, New York, 1963.
45. S. Gražulis, A. Daškevič, A. Merkys, D. Chateigner, L. Lutterotti, M. Quirós, N.R. Serebryanaya, P. Moeck, R.T. Downs, A. Le Bail, "Crystallography Open Database (COD): an open-access collection of crystal structures and platform for world-wide collaboration", *Nucleic Acids Res.*, **40** [Database issue] (2012) D420–D427.
46. A. Menad, M.E. Benmalti, A. Zaoui, M. Ferhat, "Impact of polytypism on the ground state properties of zinc oxide: A first-principles study", *Results Phys.*, **18** (2020) 103316.
47. A. Dal Corso, "Elastic constants of beryllium: a first-principles investigation", *J. Phys. Condens. Matter*, **28** [7] (2016) 075401.
48. C.J. Pickard, F. Mauri, "All-electron magnetic response with pseudopotentials: NMR chemical shifts", *Phys. Rev. B*, **63** [24] (2001) 245101.
49. M. Profeta, F. Mauri, C.J. Pickard, "Accurate first principles prediction of ^{17}O NMR parameters in SiO_2: Assignment of the zeolite ferrierite spectrum", *J. Am. Chem. Soc.*, **125** [2] (2003) 541–548.
50. A. Dal Corso, The thermo_pw software, https://dalcorso.github.io/thermo_pw.
51. L. Znaidi, "Sol-gel-deposited ZnO thin films: A review", *Mater. Sci. Eng. B*, **174** [1-3] (2010) 18–30.
52. R. Swanepoel, "Determination of surface roughness and optical constants of inhomogeneous amorphous silicon films", *J. Phys. E*, **17** [10] (1984) 896–903.

53. Filmetrics Reflectance Calculator, https://www.filmetrics.com/reflectance-calculator.
54. H. Yoshikawa, S. Adachi, "Optical constants of ZnO", *Jpn. J. Appl. Phys.*, **36** [10R] (1997) 6237–6243.
55. E.A. Alkahtani, A.E. Merad, M.R. Boufatah, A. Benosman, "DFT investigation of structural, electronic and optical properties of pure and Er-doped ZnO: Modified Becke-Johnson exchange potential", *Optik*, **128** (2017) 274–280.
56. G. Denninger, D. Reiser, "Determination of electric-field gradients in semiconductors with high precision and high sensitivity", *Phys. Rev. B*, **55** [8] (1997) 5073–5078.
57. M. Nyberg, M.A. Nygren, L.G.M. Pettersson, D.H. Gay, A.L. Rohl, "Hydrogen dissociation on reconstructed ZnO surfaces", *J. Phys. Chem.*, **100** [21] (1996) 9054–9063.
58. M. Kalay, H.H. Kart, S. Özdemir Kart, T. Çağın, "Elastic properties and pressure induced transitions of ZnO polymorphs from first-principle calculations", *J. Alloys Compd.*, **484** [1-2] (2009) 431–438.
59. N.L. Marana, S.M. Casassa, J.R. Sambrano, "Piezoelectric, elastic, infrared and Raman behavior of ZnO wurtzite under pressure from periodic DFT calculations", *Chem. Phys.*, **485-486** (2017) 98–107.
60. A.G. Every, A.K. McCurdy, *Second and Higher Order Elastic Constants - Elastische Konstanten zweiter und höherer Ordnung* (Landolt-Börnstein series, vol 29), Springer, Berlin,1993.
61. G. Carlotti, D. Fioretto, G. Socino, E. Verona, "Brillouin scattering determination of the whole set of elastic constants of a single transparent film of hexagonal symmetry", *J. Phys. Condens. Matter*, **7** [48] (1995) 9147–9153.